Au/NiCo$_2$O$_4$/3D HPG (Three-Dimensional Hierarchical Porous Graphene) Composite as Electrocatalyst for Glycerol Electrooxidation in Alkaline Medium

Bo-Cai Liu[1], Wei-Yan Xia[2], Shang-Qing Wang[1], Chang-Wei Xu[1,], Zi-Li Liu[3,*]*

[1] School of Chemistry and Chemical Engineering, Guangzhou University, Guangzhou 51006, China
[2] The Experimental School Affiliated to Guangzhou College, Guangzhou 510430, China
[3] Guangzhou Key Laboratory for new energy and green catalysis, Guangzhou University, Guangzhou 51006, China
*E-mail: cwxu@gzhu.edu.cn (C.W. Xu), gzdxlzl@163.com (Z.L. Liu)

Spinel oxide NiCo$_2$O$_4$ firstly has been explored to promote activity of Au for glycerol electrooxidation, which is supported on a three-dimensional hierarchical porous graphene-like carbon (3D HPG) material. Addition NiCo$_2$O$_4$ into the Au/HPG catalyst can significantly improve the catalytic performance for glycerol oxidation. When NiCo$_2$O$_4$ is added to the Au/HPG, onset potential is more 108 mV negatively than that on the Au/HPG. Peak current density on the Au/NiCo$_2$O$_4$(wt 6:1)/HPG is 5.1 times as high as that on the Au(20wt%)/HPG. The Au/NiCo$_2$O$_4$ in this work shows a great potential as electrocatalyst for glycerol electrooxidation in alkaline medium.

Keywords: Fuel cells; Glycerol; Gold; Spine oxide; NiCo$_2$O$_4$

1. INTRODUCTION

Fuel cells have drawn more and more interest for energy and environmental consideration. More and more people focus on the development of direct alcohol fuel cells (DAFCs) with methanol as fuel, which can be used as power sources for mobile, stationary and portable application [1, 2]. However, the development of DAFCs with methanol as fuel is facing some problems. So, other alcohols such as polyhydric alcohols have been used as alternative liquid fuels. Among polyhydric alcohols, glycerol has drawn more and more attention due to its high boiling point and low toxicity compared with methanol and abundant availability in great quantities from biodiesel industry waste (ca. 10 wt% of glycerol for the transesterification reaction of vegetable oil) [3]. The direct glycerol fuel cells (DGFCs) have attracted increasing interest and the DGFCs show some advantages such as low

fuel cross-over and high power density [4–6]. Qi *et al.* reported that direct glycerol fuel cell achieves a peak power density 276.2 mW·cm^{-2}, compared with 135.1 mW·cm^{-2} of direct methanol fuel cell with PdAg/CNT (0.5 mg Pd per MEA) as anode catalyst at 80°C and ambient pressure [7].

It's well known that Pt-based catalysts have an outstandingly catalytic performance for glycerol electrooxidation [8–10]. When we and other groups focused on the development of Pt-free electrocatalysts for glycerol oxidation, the results showed that Pd-based electrocatalysts show a great catalytic performance for glycerol oxidation in alkaline media [11–15]. However, the high price and limited supply of Pt and Pd are the major barriers to the development of DGFCs. Au has drawn more and more attention because it is abundant and more available than Pt and Pd on the earth [16–18]. The strongly adsorbed intermediate species such as CO on the surface of Pt and Pd electrodes for fuel cells poison the catalysts. Au is an excellent catalyst for CO oxidation in alkaline media. We and Habibi' group have studied the activity and stability of glycerol electrooxidation on the Au-based catalysts in alkaline media [19,20]. Our previous results showed that glycerol shows a remarkable stability on the Au electrode [19]. The results demonstrated that the CO is a promoter for glycerol oxidation on the Au/C electrode. A decay is 50% in the present of CO on the Pt/C electrode and CO will remarkably poison the Pt/C catalyst. However the current promotion on the Au/C electrode is 14% in the present CO.

Oxides such as MnO_2, CeO_2, MnO_2, Mn_3O_4, NiO, Co_3O_4 and TiO_2 have been used to enhance the activity of Pt and Pd for glycerol electrooxidation [21–24]. Oxides such as CeO_2, MnO_2, Mn_3O_4, NiO and Co_3O_4 have been used to enhance Au activity for glycerol oxidation [19,25,26]. Our previous results showed that $Au/CeO_2/C$ has great anti-poisoning effect on CO and is a more stable catalyst than the E-TEK Pt/C for glycerol oxidation in presence of CO [19]. The results showed that a current promotion on the Au/C electrode is 100% in the present CO. Padayachee *et al.* have reported the effect of adding MnO_2 to gold-based catalysts for glycerol electrooxidation and the results showed that MnO_2 may act as an active co-catalyst by oxygen spillover onto gold, which leads to higher activity and lower oxidation potential [26]. Among all the oxides to enhance the activity of Pt, Pd and Au for alcohol oxidation, cobalt oxide and nickel oxide have drawn particular attention because they can remarkably enhance the activity [27–29]. The spinel oxide $NiCo_2O_4$ has been used as catalyst for electrooxidation of methanol [30–33], ethanol [34–36] and ethylene glycol [34]. However, the activity of spinel oxide for alcohol electrooxidation is very low and negligible compared with that of Pt, Pd and Au. However, the addition $NiCo_2O_4$ into the Pt, Pd and Au will result in the activity of Pt, Pd, Au to disappear for methanol and ethanol oxidation [37]. Gao *et al.* have studied the activity of Au nanoparticle-decorated $NiCo_2O_4$ nanoflower for methanol oxidation [37]. However, the onset potential for methanol oxidation on the $Au/NiCo_2O_4$ composite electrode is approximately 0.31 V (*vs.* SCE), which is almost as the same as that on the $NiCo_2O_4$ (0.34 V) electrode in 1.0 mol·L^{-1} KOH with 0.5 mol·L^{-1} methanol. The current on the $Au/NiCo_2O_4$ electrode is just 1.3 times as high as that on the $NiCo_2O_4$ electrode. All the results show that the activity of $Au/NiCo_2O_4$ is almost same as that of $NiCo_2O_4$.

Here we will firstly use the $NiCo_2O_4$ to enhance the activity of Au for glycerol electrooxidation and also firstly use spinel oxide to enhance the activity of Pt, Pd and Au for alcohol electrooxidation.

Carbon materials are the supporting materials for electrocatalysts of glycerol electrooxidation

[38,39]. Now, graphene with monolayer or multilayers nanosheets has high specific surface area, high electronic conductivity, remarkable chemical and electrochemical stability, so the graphene-based carbon materials are expected to become new-generation supporting materials for the electrocatalysts for glycerol electrooxidation [40,41]. Kim *et al.* have reported highly dispersed PtRu nanoparticles on graphene, which show excellent activity and stability compared with Pt/C and PtRu/C for glycerol electrooxidation [42]. However, the irreversible aggregation of graphene nanosheets leads to a seriously reduced performance due to the strong van der Waals forces among individual sheet of graphene. Currently, three-dimensional (3D) graphene architecture has effective self-supporting structure to prevent aggregating of graphene sheets [43–45]. Using an efficient ion-exchange-assisted synthesis method, Shen *et al*. have got a new three-dimensional hierarchical porous grapheme-like carbon (3DHPG) material with controllable hierarchical porous structure [43]. The 3D HPG material is an outstanding support material because of high electrical conductivity, good electrochemical stability, high specific surface area. The 3D HPG material can provide an structure with a large surface area to support the oxide nanoparticles and enhance mechanical strength to suppress the aggregation of oxide nanoparticles during electrochemical process [46]. Here, $Au/NiCo_2O_4$ supported on the 3D HPG material will be studied as electrocatalyst for glycerol electrooxidation.

2. EXPERIMENTAL

2.1 Materials preparation

Glycerol, KOH, $Co(NO_3)_2 \cdot 6H_2O$, $Ni(NO_3)_2 \cdot 6H_2O$ solution(50 wt%), $HAuCl_4$, $NaBH_4$ in this work were of analytic grade purity and purchased from Aladdin. The 3D HPG was synthesized by a one-step ion-exchange/activation combination method using a cheap metal ion exchanged resin as a carbon precursor according to the Li method [43,47]. $NiCo_2O_4$/HPG was prepared as following method. $Ni(NO_3)_2 \cdot 6H_2O$ of 1.0 mmol, $Co(NO_3)_2 \cdot 6H_2O$ of 2.0 mmol and 0.4811 g HPG were added into 40 mL H_2O, then 5.0 mmol NH_4F and 12.0 mmol urea were added. After constant vigorous magnetic stirring for 1.0 h, the mixture was putted into a Teflon-lined stainless steel autoclave, then heated to 393 K for 6.0 h. The precipitate product was washed with deionized water until pH of the filtrate became 7, then dried in a vacuum oven for 12.0 h. Finally the product powder was heated at 673 K for 2.0 h in air. The $Au/NiCo_2O_4$/HPG electrocatalysts were obtained by reduction $HAuCl_4$ on the $NiCo_2O_4$/HPG powders using an excess 0.01 mol·L^{-1} $NaBH_4$ solution.

2.2 Electrode preparation

The electrocatalyst powder with 5 wt% PTFE (polytetrafluoroethylene) was dispersed in deionized water on the surface of a graphite rod with a geometric area of 0.33 cm^2. The loading of Au, carbon black and PTFE on the electrodes was controlled at 0.1, 0.23 and 0.1 mg·cm^{-2}.

2.3 Characterization

X-ray diffraction (XRD) was carried out by a powder X-ray diffractometer (Panalytical X'Pert) with Cu Kα radiation (λ=0.15418 nm). Scanning electron microscopy (SEM) images were obtained by a Quanta 400 FEG microscope (FEI Company). Transmission electron microscopy (TEM) images were obtained by a JEOL JEM-2010 (JEOL Ltd.). Raman spectroscopic images were obtained by a Raman spectrometer (Renishaw Corp., UK) using a He–Ne laser with a wavelength of 514.5 nm. X-ray photoelectron spectroscopy (XPS) images were obtained by an ESCALAB 250 spectrometer under vacuum (about 2×10^{-9} mbar).

All electrochemical measurements were carried out using solartron 1287 electrochemical work station using a standard three-electrode cell at 298 K. Solutions were freshly prepared before each experiment. A platinum foil (3.0 cm^2) and a saturated calomel electrode (SCE, 0.241 V versus SHE) were used as counter electrode and reference electrode. A salt bridge was used between the cell and reference electrode.

3. RESULTS AND DISCUSSION

Morphology of the 3D HPG was characterized by *SEM* as shown in Figure 1. The Figure 1a shows a unique 3D interconnected macroporous structure. The magnified SEM (Figure 1b) shows that 3D HPG has thin layer graphene-like walls. The TEM images further show that the HPG material has an interconnected 3D porous structure network (Figure 1c). The thin layer graphene-like wall is generally 4-6 nm thick as in Figure 1d.

XRD pattern for the Au/HPG, NiCo$_2$O$_4$/HPG, Au/NiCo$_2$O$_4$(wt 6:1)/HPG are same with our previous results [47]. Diffraction peak at around 26.4° is correspond to the (002) facet of graphene. The strong diffraction peaks for the Au/HPG at around 38.1, 44.4, 64.5 and 77.5° are correspond to the (111), (200), (220) and (311) facets of the face-centered-cubic (fcc) crystallite Au. The strong diffraction peaks for the NiCo$_2$O$_4$/HPG at around 31.4, 36.7, 44.3, 59.1 and 64.6° are correspond to the (220), (311), (200), (511) and (440) facets of the NiCo$_2$O$_4$. All the XRD pattern peaks of Au and NiCo$_2$O$_4$ can be found in the XRD image for the Au/NiCo$_2$O$_4$(wt 6:1)/HPG, which exhibits the Au/NiCo$_2$O$_4$/HPG has been synthesized successfully.

In the XRD pattern of Au/NiCo$_2$O$_4$(wt 6:1)/HPG, the diffraction peaks of Au and NiCo$_2$O$_4$ can be discovered, which indicates that the Au/NiCo$_2$O$_4$/HPG catalysts have been synthesized successfully. Chemical bonding states in the NiCo$_2$O$_4$/HPG were analyzed by XPS as shown in Figure 2. A survey spectrum of the NiCo$_2$O$_4$/HPG is shown in Figure 2a and the peaks are correspond to to binding energy peaks for C 1s, O 1s, Co 2p and Ni 2p. The binding energy value of C 1s is at 285.2 eV as shown in Figure 2a, which is related to the graphitic carbon in the 3D HPG. The binding energy values of Ni 2p are 856.6 and 874.6 eV as shown in Figure 2c, which can be correspond to that of the Ni 2p$_{3/2}$ and Ni 2p$_{1/2}$. The chemical bonding state can be assigned to Ni^{2+}, while the satellite peaks at 862.1 and 880.6 eV are two shake-up type peaks at the higher binding energy side of peaks for the Ni 2p$_{1/2}$ and Ni 2p$_{3/2}$ edge [48,49]. The Ni 2p spectra for the two spin-orbit doublet characteristics of Ni^{2+} with low content

of Ni^{3+} are consistent with two shake-up satellite peaks [37]. The binding energy values of Co 2p are 780.6 and 797.6 eV for the $NiCo_2O_4$/HPG assigned to that of the Co $2p_{3/2}$ and Co $2p_{1/2}$ as shown in Figure 2d, which can be correspond to Co^{3+} with low content of Co^{2+} [37,49]. The results indicate that the $NiCo_2O_4$/HPG has been synthesized successfully.
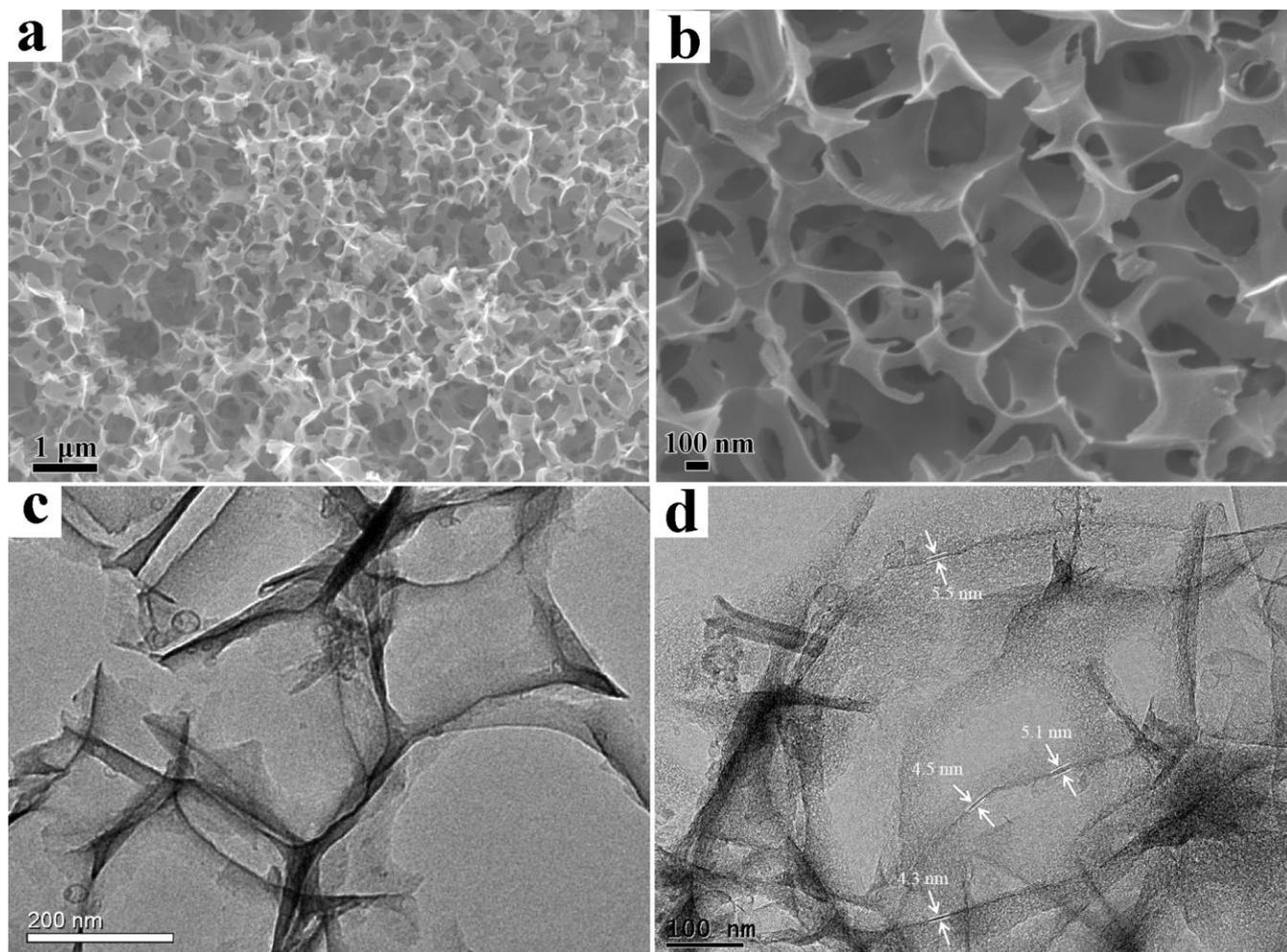

Figure 1. (a,b) SEM images and (c,d) TEM of 3D HPG.

The graphitization degree of the HPG was characterized by Raman spectroscopic image, which has been reported in our previous results [47]. The ratio of the peak intensity of D band for crystalline graphene layers to that of G band for disordered carbon (I_D/I_G) is 1.05 for the HPG. The value of I_D/I_G for the $NiCo_2O_4$/HPG is a little lower than that for the HPG. It may be related to the $NiCo_2O_4$ supported on the surface of the HPG, which leads to decrease graphitic defects in the HPG [50].

A survey XPS spectrum for the Au/$NiCo_2O_4$(wt 6:1)/HPG is shown in Figure 2a and the peaks are correspond to binding energy peaks for Au 4f, C 1s, O 1s, Co 2p and Ni 2p. The binding energy values of Au 4f are 84.2 and 88.1 eV as shown in Figure 2b, which can be assigned to the Au $4f_{5/2}$ and Au $4f_{7/2}$, and are typical binding energy values of metallic Au^0 [51]. The result shows that Au supported on the surface of $NiCo_2O_4$/HPG. The binding energy values of Ni 2p are 857.0 and 876.6

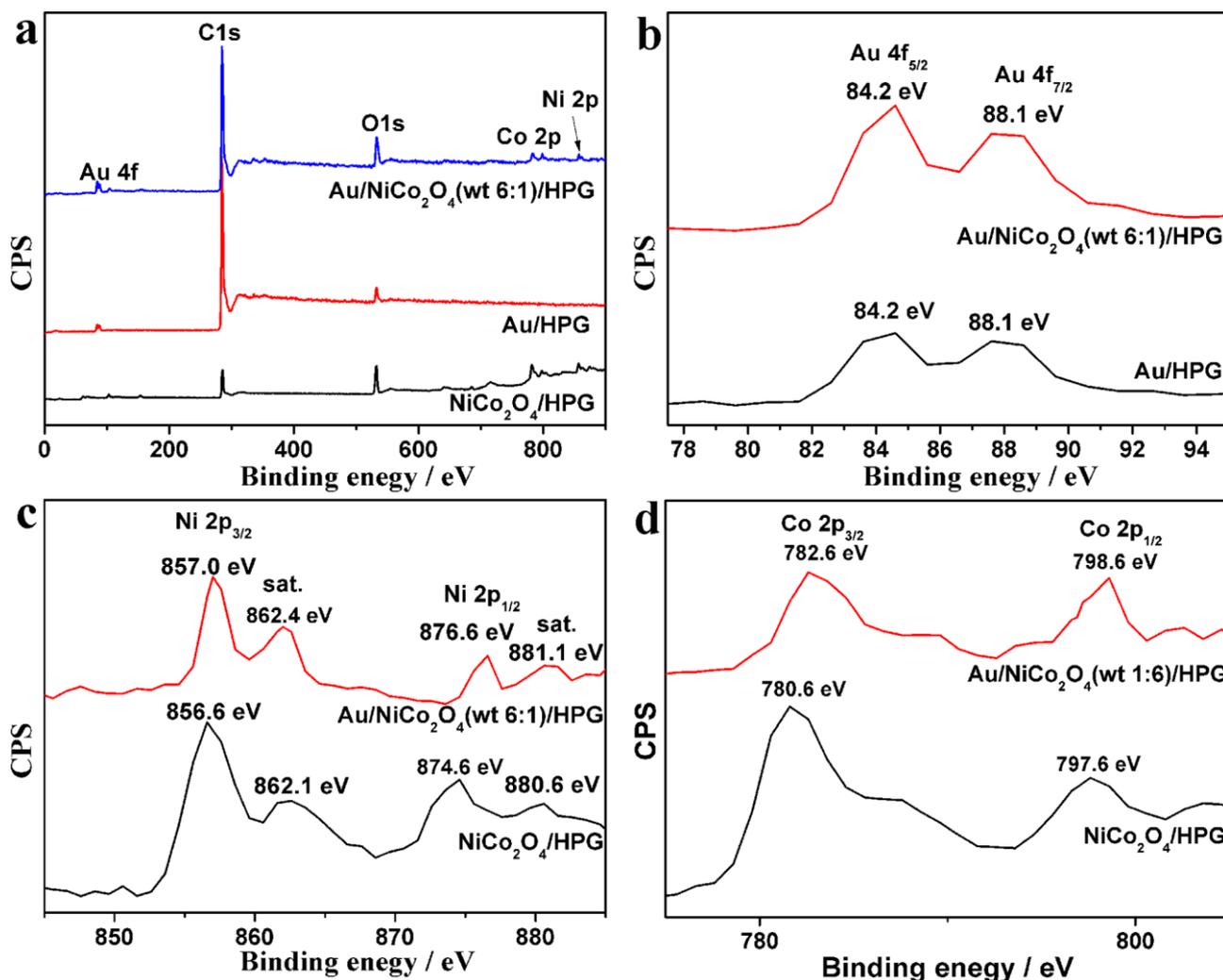eV as shown in Figure 2c, which can be assigned to the Ni $2p_{3/2}$ and Ni $2p_{1/2}$, and are assigned to that of Ni^{2+}.

Figure 2. XPS spectra for $Au/NiCo_2O_4$(wt 6:1)/HPG of (a) survey, (b) Au 4f, (c) Ni 2p and (d) Co 2p.

The Ni 2p spectrum for the two spin-orbit doublet characteristics of Ni^{2+} with low content of Ni^{3+} is consistent with two shakeup satellites. The binding energy values of Co 2p are 782.6 and 798.6 eV for the $Au/NiCo_2O_4$(wt 6:1)/HPG assigned to the Co $2p_{3/2}$ and Co $2p_{1/2}$ as shown in Figure 2d, which can be assigned to Co^{3+} with low content of Co^{2+}. In the XPS spectrum of $Au/NiCo_2O_4$(wt 6:1)/HPG, the binding energy values of Au and $NiCo_2O_4$ can be discovered, which indicates that the $Au/NiCo_2O_4$/HPG catalysts have been synthesized successfully.
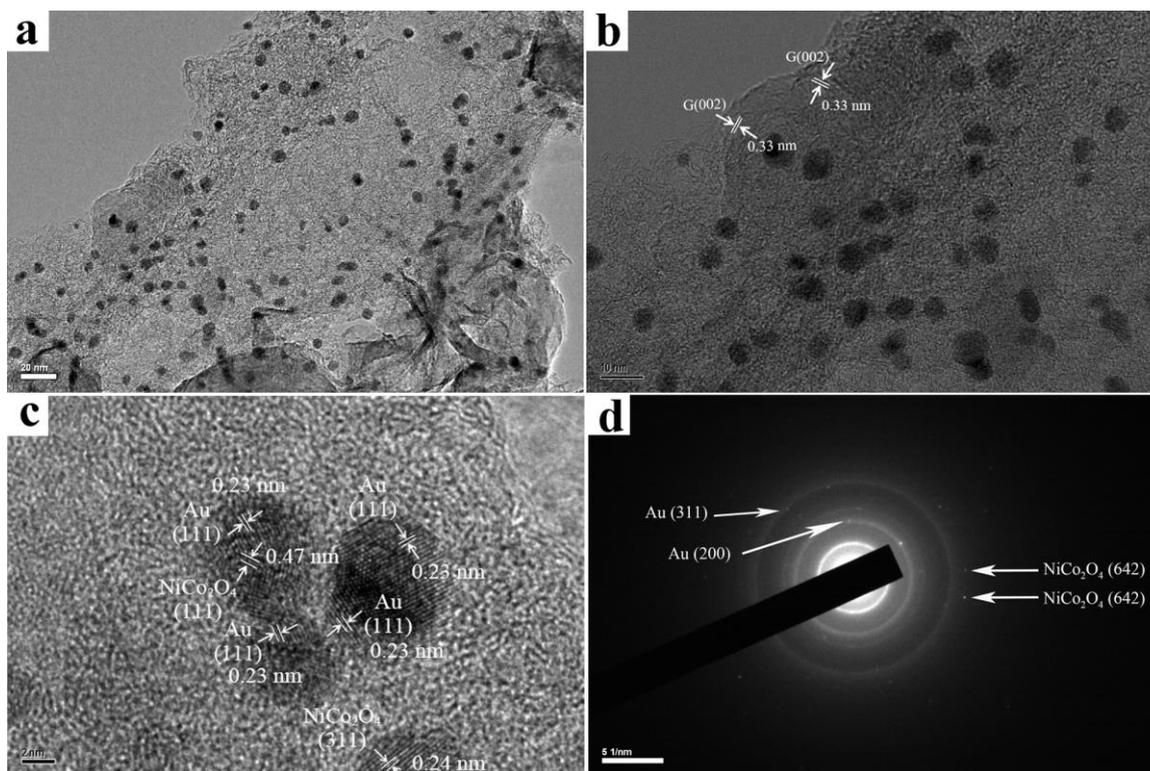
Figure 3. (a,b) TEM images, (c) HRTEM image and (d) SAED) pattern for Au/NiCo$_2$O$_4$(wt 6:1)/HPG.

The typical TEM images of the Au/NiCo$_2$O$_4$(wt 6:1)/HPG are shown in Figure 3. The nanocatalyst particles have a narrow sized distribution of 2-6 nm and they are well dispersed on the surface of 3D HPG (Figure 3a and Figure 3b). A parallel fringe with a 0.33 nm space can be correspond to the (002) facet of graphene (Figure 3b). The parallel fringes with spaces of 0.47 and 0.24 nm are correspond to the (111) and (311) facets of the NiCo$_2$O$_4$ and the parallel fringe with a 0.23 nm space is correspond to the (111) plane of Au as shown in Figure 3c. From the TEM images, the nanoparticles of NiCo$_2$O$_4$ and Au can be clearly seen to contact each other or exit in one particle. The selected area electron diffraction (SAED) pattern of the Au/NiCo$_2$O$_4$(wt 6:1)/HPG shows a set of well-defined rings for face-centered-cubic (fcc) crystallite Au and spinel NiCo$_2$O$_4$, indicating its polycrystalline structure as shown in Figure 3d.

Cyclic voltammetry (CV) measurement for glycerol electrooxidation on the NiCo$_2$O$_4$/HPG electrode is carried out in 1.0 mol·L^{-1} KOH containing 1.0 mol·L^{-1} glycerol solution with a sweep rate of 5 mV·s^{-1} at a NiCo$_2$O$_4$ loading of 0.10 mg·cm^{-2} to evaluate the activity of NiCo$_2$O$_4$ as shown in inset figure of Figure 4a. The background is the CV measured in a nitrogen-saturated 1.0 mol·L^{-1} KOH solution without glycerol on the NiCo$_2$O$_4$/HPG electrode. Compared with the CV in the absence of glycerol, a glycerol oxidation peak can be clearly observed in the CV curve on the NiCo$_2$O$_4$/HPG electrode in the presence of 1.0 mol·L^{-1} glycerol. The onset potential (E_{onset}) is 0.232 V on the NiCo$_2$O$_4$/HPG electrode. This results is very as similar with that reported by Sun *et al.* for methanol, ethanol and ethylene glycol [34,52]. The E_{onset} is about 0.48 V *vs.* Hg/HgO(1.0 mol·L^{-1} KOH) for ethanol and ethylene glycol, 0.536 V for methanol in 1.0 mol·L^{-1} KOH and 0.5 mol·L^{-1} alcohol (methanol, ethanol or ethylene glycol) at 10 mV·s^{-1}. In the forward scan in the CV curve, oxidation

current is correspond to the oxidation of freshly chemisorbed species from glycerol adsorption, so the magnitude of oxidation current indicates the activity of electrocatalyst for glycerol oxidation. A glycerol oxidation current can be observed in the CV curve on the Au(20wt%)/HPG electrodes in the Figure 4a. It is obviously that the activity of glycerol oxidation on the Au(20wt%)/HPG electrode is much higher than that on the Au(20wt%)/C (Carbon Vulcan XC-72) electrode [25]. The E_{onset} is -0.412 V on the Au(20wt%)/HPG electrode, which is 157 mV more negative compared with that on the Au(20wt%)/C electrode (-0.255 V). The lower value of E_{onset} shows easier electrooxidation of glycerol. The current for glycerol electrooxidation on the Au(20wt%)/HPG electrode begins to rise much more sharply at more negative potential than that on the Au(20wt%)/C electrode. It demonstrates that glycerol can be easily electrochemically oxidized on the Au(20wt%)/HPG electrode. Current density at the potential of -0.3 V ($j_{-0.3V}$) is 1.8 mA·cm^{-2} on the Au(20wt%)/HPG electrode, which is 2.3 times as high as that on the Au(20wt%)/C electrode, which is 0.8 mA·cm^{-2}. The results show that the HPG is a good support for electrocatalysts for glycerol oxidation.
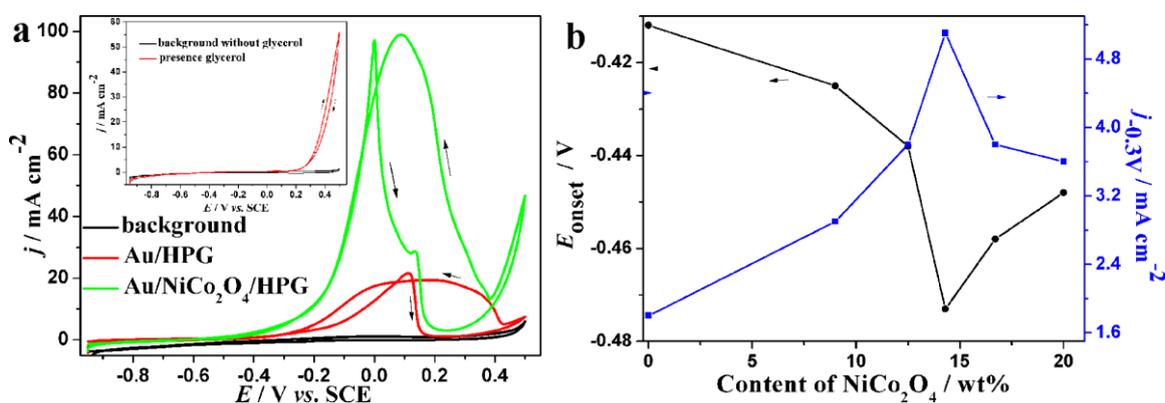

Figure 4. (a) CV curves on the NiCo$_2$O$_4$/HPG, Au/HPG and Au/NiCo$_2$O$_4$(wt 6:1)/HPG electrodes in 1.0 mol·L^{-1} KOH containing 1.0 mol·L^{-1} glycerol with a sweep rate of 5 mV·s^{-1} (The inset figure is CV curve on NiCo$_2$O$_4$/HPG electrode in 1.0 mol·L^{-1} KOH containing 1.0 mol·L^{-1}), (b) Plots of E_{onset} and $j_{-0.3V}$ in CV curves as a function of the Au weight percent in Au/NiCo$_2$O$_4$.

CV measurement for glycerol electrooxidation on the Au/NiCo$_2$O$_4$(wt 6:1)/HPG electrode is carried out in 1.0 mol·L^{-1} KOH containing 1.0 mol·L^{-1} glycerol solution with a sweep rate of 5 mV·s^{-1} at a Au loading of 0.10 mg·cm^{-2} as shown in Figure 4a. A glycerol oxidation peak can be clearly observed in the CV curve on the Au/NiCo$_2$O$_4$(wt 6:1)/HPG electrode. It is obviously that the activity of glycerol oxidation on the Au/NiCo$_2$O$_4$(wt 6:1)/HPG electrode is much higher than that on the Au(20wt%)/HPG electrode. The E_{onset} is -0.520 V on the Au/NiCo$_2$O$_4$(wt 6:1)/HPG electrode, which is 108 mV more negative compared with that on the Au(20wt%)/HPG electrode (-0.412 V). The current for glycerol electrooxidation on the Au/NiCo$_2$O$_4$(wt 6:1)/HPG electrode begins to rise much more sharply at more negative potential than that on the Au(20wt%)/HPG electrode. It demonstrates that glycerol can be easily electrochemically oxidized on the Au/NiCo$_2$O$_4$(wt 6:1)/HPG electrode. Glycerol has a high value of E_{onset} on the Au(20wt%)/HPG, so it is difficult to be electrochemically oxidized on pure Au electrocatalyst. When NiCo$_2$O$_4$ is added to the Au/HPG, the value of E_{onset} is 108 mV more negative. The peak current density (j_p) is 99.2 mA·cm^{-2} (0.088 V) on the Au/NiCo$_2$O$_4$(wt 6:1)/HPG

electrode, which is 5.1 times as high as that on the Au(20wt%)/HPG electrode, which is 19.3 mA·cm^{-2} (0.160 V). The value of $j_{-0.3V}$ is 5.1 mA·cm^{-2} on the Au/NiCo$_2$O$_4$(wt 6:1)/HPG electrode, which is 2.8 times as high as that on the Au(20wt%)/HPG electrode, which is 1.8 mA·cm^{-2}. The results show that NiCo$_2$O$_4$ can promote activity of Au for glycerol oxidation.

The effect of NiCo$_2$O$_4$ content on the Au/NiCo$_2$O$_4$/HPG electrocatalysts for glycerol oxidation was investigated in a N$_2$-saturated 1.0 mol·L^{-1} KOH + 1.0 mol·L^{-1} glycerol solution with a sweep rate of 5 mV·s^{-1}. Au loading was fixed as 0.10 mg·cm^{-2}. Figure 4b shows the plots of value of E_{onset} and $j_{-0.3V}$ as a function of NiCo$_2$O$_4$ loading for glycerol oxidation. It can be seen that value of E_{onset} for glycerol oxidation decreases with increase of oxide content in the Au/NiCo$_2$O$_4$/HPG catalysts, but increases again when value of E_{onset} reaches a minimum value. Meanwhile, the value of $j_{-0.3V}$ for glycerol oxidation increases with increase of NiCo$_2$O$_4$ content in the Au/NiCo$_2$O$_4$/HPG catalysts, but decreases again when it reaches a maximum value. The best result is found as weight ratio 6:1 for Au to NiCo$_2$O$_4$ in the Au/NiCo$_2$O$_4$/HPG with the lowest onset potential and the highest current density on the potential of -0.3 V.
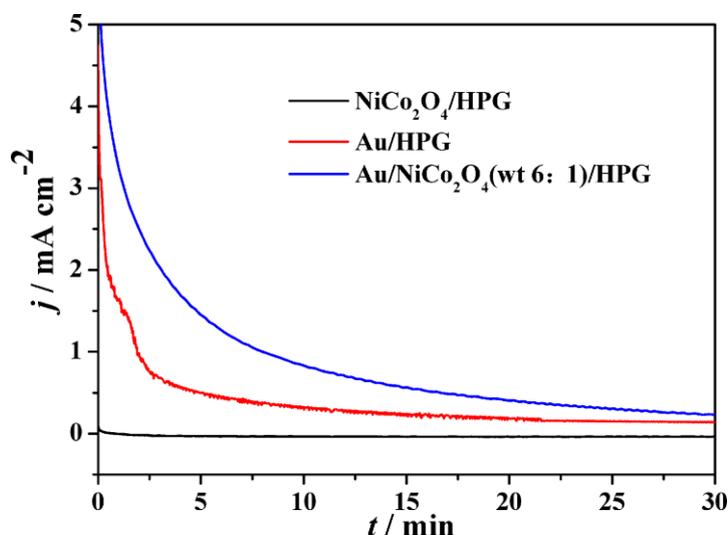

Figure 5. Chronoamperomety curves on NiCo$_2$O$_4$/HPG, Au/HPG and Au/NiCo$_2$O$_4$(wt 6:1)/HPG electrodes in 1.0 mol·L^{-1} KOH containing 1.0 mol·L^{-1} glycerol at a potential of -0.3 V.

The chronoamperometry curves from -0.6 to -0.3 V for glycerol oxidation on the NiCo$_2$O$_4$/HPG, Au/HPG and Au/NiCo$_2$O$_4$(wt 6:1)/HPG electrodes in 1.0 mol·L^{-1} KOH solution containing 1.0 mol·L^{-1} glycerol are shown in Figure 5. It is well-known that the strongly adsorbed intermediates during glycerol electrooxidation such as acyl species (-CO$_{ads}$) will be adsorbed and block the electrode surface, then the current of glycerol oxidation will decrease. The rapid current decay in the chronoamperometry curves shows a catalyst poison. The current decays rapidly on the Au/HPG electrode, while the current decays slowly on the Au/NiCo$_2$O$_4$(wt 6:1)/HPG electrodes. The results show that the NiCo$_2$O$_4$ can enhance the stability of the Au/HPG for glycerol oxidation. Nevertheless, at the end of the test, the oxidation current density is 0.24 mA·cm^{-2} on the Au/NiCo$_2$O$_4$(wt 6:1)/HPG electrode which is larger than that on the Au/HPG electrode (0.15 mA cm^{-2}).

The promoted electrochemical performance of glycerol oxidation on the $Au/NiCo_2O_4/HPG$ catalyst can be attributed to a bifunctional mechanism. Glycerol electrooxidation on the Au electrode needs both free surface and oxygen-containing species (OH_{ads}) on the surface of Au [53,54]. However, the free surface on the Au electrode could decrease by two main causes, which are the Au oxide formation and the adsorption of reaction intermediates. It is believed that oxides like $NiCo_2O_4$, have capacity to generate active OH_{ads} on the Au surface at a lower potential [53,26]. The strongly adsorbed intermediate species on the surface of electrode at lower potential can reaction with oxygen-containing species to species dissolved in water, which will make free surface and active sites for further electrochemical reaction on the electrode [55].

4. CONCLUSIONS

An active three-dimensional hierarchical porous graphene-like carbon (3D HPG) material has been prepared using an efficient ion-exchange-assisted synthesis route. The results show that the HPG is a good support for electrocatalysts for glycerol oxidation. It is obviously that the activity of glycerol oxidation on the Au(20wt%)/HPG electrode is much higher than that on the Au(20wt%)/C (Carbon Vulcan XC-72) electrode. The preliminary results indicate that the addition $NiCo_2O_4$ into the Au/HPG catalyst can significantly improve the electrochemical performance for glycerol oxidation. When $NiCo_2O_4$ is added to the Au/HPG, the value of E_{onset} is more 108 mV negatively than that on the pure Au/HPG catalyst. The value of $j_{-0.3V}$ on the $Au/NiCo_2O_4$(wt 6:1)/HPG electrode is 2.8 times as high as that on the Au(20wt%)/HPG electrode. The activity and stability of glycerol oxidation on the Au/HPG are promoted obviously by addition of $NiCo_2O_4$. The $Au/NiCo_2O_4$ presented in this work may be a potential as good electrocatalyst with low price for glycerol electrooxidation in alkaline medium in direct glycerol fuel cells.

References

1. V. Mandanipour, M. Noroozifar and A. R. Modarresi-Alam, *Int. J. Electrochem. Sci.*, 11 (2016) 5302.
2. G. F. Xu, Z. F. Li, S. W. Wang and X. J. Yu, *J. Power Sources*, 195 (2010) 4731.
3. A. Zalineeva, A. Serov, M. Padilla, U. Martinez, K. Artyushkova, S. Baranton, C. Coutanceau and P. B. Atanassov, *Appl. Catal. B: Environ.*, 176–177 (2015) 429.
4. A. N. Geraldes, D. F. da Silva, L. G. D. E. Silva, E. V. Spinace, A. O. Neto and M. C. dos Santos, *J. Power Sources*, 293 (2015) 823.
5. N. Benipal, J. Qi and J. C. Gentile, *Renew. Energy*, 105 (2017) 647.

6.   Z. Y. Zhang, L. Xin and W. Z. Li, *Appl. Catal. B: Environ.*, 119 (2012) 40.
7.   J. Qi, N. Benipal, C. H. Liang and W. Z. Li, Appl. Catal. B: Environ., 199 (2016) 494.
8.   L. Huang, *et al.*, *ACS Catal.*, 6 (2016) 7686.
9.   C. A. Ottoni, C. E. D. Ramos, R. F. B. de Souza, S. G. da Silva, E.V. Spinace and A. O. Neto, *Int. J. Electrochem. Sci.*, 13 (2018) 1893.
10. A. J. Xie, *et al.*, *Electrochim. Acta*, 231 (2017) 502.
11. P. K. Shen and C. W. Xu, *Electrochem. Commun.*, 8 (2006) 184.
12. C. W. Xu, Z. Q. Tian, P. K. Shen and S. P. Jiang, *Electrochim. Acta*, 53 (2008) 2610.
13. C. A. Ottoni, S. G. da Silva, R. F. B. de Souza and A. O. Neto, *Ionics*, 22 (2016) 1167.
14. R. Wang, L.Y. Jiang, J. J. Feng, W. D. Liu, J. H. Yuan and A. J. Wang, *Int. J. Hydrogen Energy*, 42 (2017) 6695.
15. L. Niu, Q. Zhang, S. J. Chao, M. Shi, R. M. Huang, Z. Y. Bai and L. Yang, *Ionics*, 21 (2015) 1989.
16. J. Qi, *et al.*, *Appl. Catal. B: Environ.*, 154 (2014) 360.
17. J. H. Zhang, Y. J. Liang, N. Li, Z. Y. Li, C. W. Xu and S. P. Jiang, *Electrochim Acta*, 59 (2012) 156.
18. Z. Y. Zhang, L. Xin, J. Qi, D. J. Chadderdon and W. Z. Li, *Appl. Catal. B: Environ.*, 136 (2013) 29.
19. J. H. Zhang, T. Zhu, N. Li and C. W. Xu, *J. Energy Inst.*, 89 (2016) 325.
20. E. Habibi and H. Razmi, *Int. J. Hydrogen Energy*, 37 (2012) 16800.
21. P. M. Ejikeme, K. Makgopa, K. Raju and K. I. Ozoemena, *ChemElectroChem*, 3 (2016) 2243.
22. A. C. Garcia, E. B. Ferreira, V. V. S. de Barros and J. J. Linares, *J. Electroanal. Chem.*, 793 (2017) 188.
23. Y. M. Kang, W. Wang, Y. L. Pu, J. M. Li, D. Chai and Z. Q. Lei, *Chem. Eng. J.*, 308 (2017) 419.
24. L. Su, W. Z. Jia, A. Schempf and Y. Lei, *Electrochem. Commun.*, 11 (2009) 2199.
25. Y. Z. Su, Q. Z. Xu, Q. S. Zhong, C. J. Zhang, S. T. Shi and C. W. Xu, *Mater. Res. Bull.*, 64 (2015) 301.
26. D. Padayachee, V. Golovko and A. T. Marshall, *Electrochim. Acta*, 98 (2013) 208.
27. K. H. Ye, S. A. Zhou, X. C. Zhu, C. W. Xu and P. K. Shen, *Electrochim. Acta*, 90 (2013) 108.
28. Y. Sun, *et al.*, *Nanoscale*, 9 (2017) 5467.
29. S. L. Nie, Y. C. Zhao, J. W. Fan, J. N. Tian, Z. Ning and X. X. Li, *Acta Phys-Chim. Sin.*, 28 (2012) 871.
30. W. Wang, Q. X. Chu, Y. N. Zhang, W. Zhu, X. F. Wang and X. Y. Liu, *New J. Chem.*, 39 (2015) 6491.
31. M. U. A. Prathap and R. Srivastava, *Nano Energy*, 2 (2013) 1046.
32. S. N. Sun and Z. J. Xu, *Electrochim. Acta*, 165 (2015) 56.
33. Z. S. Li, R. R. Yang, B. L. Li, M. Yu, D. H. Li and H. Q. Wang, *Electrochim. Acta*, 252 (2017) 180.
34. S. N. Sun, Y. Zhou, B. L. Hu, Q. C. Zhang and Z. J. Xu, *J. Electrochem. Soc.*, 163 (2016) H99.
35. J. Zhan, M. Cai, C. F. Zhang and C. Wang, Electrochim. Acta, 154 (2015) 70.
36. S. S. Jayaseelan, T. H. Ko, S .Radhakrishnan, C. M. Yang, H. Y. Kim and B. S. Kim, *Int. J. Hydrogen Energy*, 41 (2016) 13504.
37. H. X. Gao, Y. Cao, Y. Chen, X. Y. Lai and S. J. Ding, *J. Alloys Compd.*, 732 (2018) 460.
38. J. H. Zhang, T. Zhu, N. Li and C. W. Xu, *Int. J. Electrochem. Sci.*, 8 (2013) 9508.
39. W. Y. Yuan, J. Zhang, P. K. Shen, C. M. Li and S. P. Jiang, *Electrochim. Acta*, 190 (2016) 817.
40. C. C. Jin, J. H. Zhu, R. L. Dong and Q. S. Huo, *Electrochim. Acta*, 190 (2016) 829.
41. H. B. Wang, L. Thia, N. Li, X. M. Ge, Z. L. Liu and X. Wang, *ACS Catal.*, 5 (2015) 3174.
42. H. J. Kim, S. M. Choi, M. H. Seo, S. Green, G. W. Huber and W. B. Kim, *Electrochem. Commun.*, 13 (2011) 890.
43. Y. Y. Li , Z. S. Li and P. K. Shen, *Adv. Mater.*, 25 (2013) 2474.
44. Z. S. Wu, Y. Sun, Y. Z. Tan, S. Yang, X. L. Feng and K. Müllen, *J. Am. Chem. Soc.*, 134 (2012) 19532.
45. N. Arjona, *et al.*, *New J. Chem.*, 41 (2017) 1854.

46. Y. Y. Li, Q. W. Zhang, J. L. Zhu, X. L. Wei and P. K. Shen, *J. Mater. Chem. A*, 2 (2014) 3163.
47. W. Y. Xia, N. Li, Q. Y. Li, K. H. Ye and C. W. Xu, *Sci. Rep.*, 6 (2016) 23398. doi: 10.1038/srep23398.
48. L. Gu, L. Qian, Y. Lei, Y. Y. Wang, J. Li, H. Y. Yuan and D. Xiao, *J. Power Sources*, 261 (2014) 317.
49. E. Umeshbabu and G. R. Rao, *Electrochim. Acta*, 213 (2016) 717.
50. A. Sadezky, H. Muckenhuber, H. Grothe, R. Niessner and U. Pöschl, *Carbon*, 43 (2005) 1731.
51. E. D. Park and J. S. Lee, *J. Catal.*, 186 (1999) 1.
52. R. Dinga, L. Qi, M. J. Jia and H. Y. Wang, *Electrochim. Acta*, 113 (2013) 290.
53. S. Yongprapat, S. Therdthianwong and A. Therdthianwong, *Electrochim. Acta*, 83 (2012) 87.
54. J. F. Gomes, L. H. S. Gasparotto and G. Tremiliosi-Filho, *Phys. Chem. Chem. Phys.*, 15 (2013) 10339.
55. Z. P. Liu, P. Hu and A. Alavi, *J. Am. Chem. Soc.*, 124 (2002) 14770.